

dance. But, if we assume that the true iron abundance of the hot interstellar medium is solar, then we might be forced to infer that only 30% of the diffuse emission is actually thermal. Despite the observation of thermal line emission, it is thus difficult to rule out a component of diffuse emission from inverse Compton scattering. Assuming that the hard diffuse emission contains a major component of thermal origin (30 to 100% of the total) and integrating over the Gaussian elliptical region, we estimate that the plasma has a temperature of  $\sim T \approx 40$  MK and pressure of the order of  $P/k \approx 10^9 \text{ cm}^{-3}$ .

It seems quite likely that the hot component is not in hydrostatic equilibrium and is the basic driving force for the galactic wind outflowing perpendicular to the plane of M82. This hot x-ray-emitting gas is thus overpressurized as compared to the galaxy's gravitational potential well and is thus probably the principal driving mechanism for the hot outflow of chemically enriched material into the intergalactic medium. Such high-temperature plasmas in the cores of starburst galaxies may be the basic drivers for the chemical enrichment of the intergalactic medium and the intracluster medium within clusters of galaxies.

References and Notes

1. D. W. Weedman *et al.*, *Astrophys. J.* **248**, 105 (1981).
2. Y. Sofue, Ed., *The Central Regions of the Galaxy and Galaxies, IAU Symp. 184* (Kluwer, Dordrecht, Netherlands, 1998).
3. K. A. Van der Hucht, G. Koenigsberger, P. R. Eenens, Eds., *Wolf-Rayet Phenomena in Massive Stars and Starburst Galaxies, IAU Symp. 193* (Astronomical Society of the Pacific, San Francisco, 1999).
4. J. E. Barnes, D. B. Sanders, Eds., *Galaxy Interactions at Low and High Redshift, IAU Symp. 196* (Kluwer, Dordrecht, Netherlands, 1999).
5. S. Holt, E. Smith, Eds., *After the Dark Ages: When Galaxies Were Young* (AIP Press, New York, 1999).
6. W. Freedman *et al.* *Astrophys. J.* **427**, 628 (1994).
7. P. Kronberg, in *Galactic and Extragalactic Star Formation*, R. E. Pudritz, M. Fich, Eds. (Reidel, Boston, 1988), pp. 391–399.
8. R. E. Griffiths, M. D. Johnson, D. A. Schwartz, J. Schwarz, J. C. Blades, *Astrophys. J.* **230**, L21 (1979).
9. M. G. Watson, V. Stanger, R. E. Griffiths, *Astrophys. J.* **286**, 144 (1984).
10. J. N. Bregman, E. Schulman, K. Komisaka, *Astrophys. J.* **439**, 155 (1995).
11. T. G. Tsuru, H. Awaki, K. Koyama, A. Ptak, *Publ. Astron. Soc. Jpn.* **49**, 619 (1997).
12. E. C. Moran, M. D. Lehnert, *Astrophys. J.* **478**, 172 (1997).
13. I. R. Stevens, D. K. Strickland, K. A. Wills, *Mon. Not. R. Astron. Soc.* **308**, 123 (1999).
14. A. Ptak, R. E. Griffiths, *Astrophys. J.* **517**, L85 (1999).
15. M. C. Weisskopf, S. L. O'dell, L. P. van Speybroeck, *Proc. SPIE* **2805**, 2 (1996).
16. G. Garmire *et al.*, in preparation.
17. ACIS on the CXO provides sub-arc second imaging across a wide spectral band, low instrumental background rates permitting study of extended structures, and moderate spectral resolution at every pixel for astrophysical modeling.
18. The displayed images required several steps of data processing. With level 1-processed detected "event" lists, several types of events that were probably dominated by cosmic ray primary and secondary particles rather than imaged x-rays were removed: (i) event energies above 8 keV and below 0.2 keV; (ii) events split between pixels, except for standard ASCA grades; (iii) "hot columns" and other low-quality

- events; and (iv) brief periods of high background. The ACIS-I chips suffered radiation damage early in the Chandra mission, producing an increase in its charge-transfer inefficiency (CTI) during readout. To compensate for this effect, we recalibrated the ADU (analog-to-digital unit)-to-energy conversion for each photon as a function of its CCD pixel coordinate in the y direction (CHIPY) location using the calibration data set acisf1310. This correction is similar to that in (29) and produces individual photon energies accurate to  $\sim 10\%$ . Our analysis here concentrates on events extracted from CHIPY > 700 in CCD I3, where most of the events detected from M82 are found. The resulting count-rate map was subject to adaptive kernel smoothing, which permits simultaneous viewing of compact and extended structures (29). Point sources were located with a multiscale wavelet analysis of the image (30). Although this procedure reliably detects isolated sources down to about seven photons, its sensitivity within the bright diffuse emission pervading the core of M82 is lower and difficult to determine quantitatively.
19. A. Collura, F. Reale, E. Schulman, J. N. Bregman, *Astrophys. J.* **420**, L63 (1994).
20. G. H. Rieke, M. J. Lebovsky, R. I. Thompson, F. J. Low, A. T. Tokunaga, *Astrophys. J.* **238**, 24 (1980).
21. D. Barret, J. E. McClintock, J. E. Grindlay, *Astrophys. J.* **473**, 963 (1996).
22. K. A. Wills, A. Pedlar, T. W. B. Muxlow, I. R. Stevens, *New Astron. Rev.* **43**, 633 (1999).
23. R. W. O'Connell, J. S. Gallagher, D. A. Hunter, W. N. Colley, *Astrophys. J.* **446**, L10 (1995).
24. L. Townsley *et al.*, in preparation.
25. These fits were performed with XIMGFIT, which is available at <http://snooper.phys.cmu.edu/ximgfit>. Photons from the sources in Table 1 were removed

- by replacing pixels where the contrast between the source model (Gaussian) and background model exceeded 50% by a Poisson deviate with a mean value given by the background model at that position.
26. H. V. D. Bradt, J. E. McClintock, *Annu. Rev. Astron. Astrophys.* **21**, 13 (1983).
27. A. P. Cowley *et al.*, in *The Stellar Content of Local Group Galaxies, IAU Symp. 192*, P. A. Whitelock, R. D. Cannon, Eds. (Astronomical Society of the Pacific, San Francisco, 1999), pp. 100–103.
28. We caution that the calibration of the ACIS spectral response is still evolving because of the CTI problem (18), and spectral fitting for extended structures is likely to improve beyond the work presented here.
29. L. Townsley *et al.*, *Astrophys. J.* **534**, L139 (2000).
30. H. Ebeling, D. A. White, V. N. Rangarajan, *Mon. Not. R. Astron. Soc.*, in press.
31. R. W. O'Connell, J. J. Mangano, *Astrophys. J.* **221**, 62 (1978).
32. P. E. Freeman, V. Kashyap, R. Rosner, D. Q. Lamb, in preparation.
33. H. Kaneda *et al.*, *Astrophys. J.* **491**, 638 (1997).
34. S. Satyapal *et al.*, *Astrophys. J.* **483**, 148 (1997).
35. Z. P. Huang, T. X. Thuan, R. A. Chevalier, J. J. Condon, Q. F. Yin, *Astrophys. J.* **424**, 114 (1994).
36. R. de Grijs, R. W. O'Connell, G. D. Becker, R. A. Chevalier, J. S. Gallagher III, *Astron. J.* **119**, 68 (2000).
37. We express our appreciation for the many scientists and engineers who brought Chandra to fruition, in particular those at the Massachusetts Institute of Technology, Penn State University, and Lockheed Martin who contributed to the ACIS instrument. This research was funded by NASA contract NAS8-38252 to Penn State University.

27 July 2000; accepted 10 October 2000

## Defect-Induced Phase Separation in Dipolar Fluids

T. Tlusty\* and S. A. Safran\*

A defect-induced, critical phase separation in dipolar fluids is predicted, which replaces the usual liquid-gas transition that is driven by the isotropic aggregation of particles and is absent in dipolar fluids due to strong chaining. The coexisting phases are a dilute gas of chain ends that coexists with a high-density liquid of chain branching points. Our model provides a unified explanation for the branched structures, the unusually low critical temperature and density, and the consequent two-phase coexistence "islands" that were recently observed in experiment and simulation.

The critical liquid-gas phase transition (LGT) is a generic feature of simple fluids. When the temperature is decreased below the critical temperature, the simple fluid phase separates into a low-density gas that coexists with a high-density liquid. The phase separation is well understood as the consequence of a temperature-dependent interplay between the entropy loss due to hard-core repulsion and a short-range isotropic attraction, as was first formulated by van der Waals in his equation of state. In contrast, the basic thermodynamics of di-

polar fluids, where the attraction is due to long-range anisotropic dipolar forces, are still obscure, including the basic question of whether the LGT exists at all.

Dipolar fluids have numerous scientific and industrial applications, mostly related to the strong field-responsive properties of colloidal ferrofluids (1) or electro-rheological fluids (2). For these applications, it is crucial to know whether the system exists in a single homogenous phase. Dipolar fluids also have theoretical significance as a fundamental model of statistical mechanics, perhaps the simplest example of an anisotropic fluid, which may provide physical insight for polar fluids such as hydrogen fluoride or even water.

The mean dipolar interaction between two particles is attractive (with a Boltz-

Department of Materials and Interfaces, Weizmann Institute of Science, Rehovot, Israel.

\*To whom correspondence should be addressed. E-mail: cptsvi@weizmann.ac.il (T.T.); sam.safran@weizmann.ac.il

mann weighted average due to mutual orientation), which may lead one to conclude within a mean-field theory that a LGT similar to that exhibited by isotropic fluids should also occur in dipolar fluids (3). However, simulation studies (4–7) reveal a completely different and more complex scenario: The anisotropic dipolar interaction, which favors a nose-to-tail alignment of the dipoles (Fig. 1A), drives the particles to self assemble in polymer-like chains (Fig. 1B) (8, 9). The linear aggregation of the chains is a one-dimensional process in which no phase transition is expected to occur. The absence of the LGT has been attributed to the strong chaining that interferes with the isotropic aggregation (7, 10–12).

Large-scale computer simulations have found evidence for the occurrence of a critical liquid-gas transition in a system of hard spheres with solely dipolar interactions (13); however, the estimated critical temperature and density are unusually low in comparison to simple fluid values. In the proximity of the critical point, the simulated dipolar spheres assemble in chains with apparent branching points. Thermodynamic measurements found evidence for a critical liquid-gas transition in magnetic fluids consisting of ferric oxide nanospheres (14). However, in this colloidal fluid it is difficult to separate the effect of the dipolar interaction from the short-range isotropic attraction (15).

Motivated by these experimental and simulation studies, we consider a model whose basic components are not the dipolar spheres themselves but the ensemble of self-assembling chains they form, allowing us to focus on the collective large-scale features of the system. The dipolar fluid consists of identical spheres of diameter  $D$  carrying a magnetic moment of amplitude  $\mu$ . The dipolar interaction between two spheres whose dipoles are  $\vec{\mu}_1, \vec{\mu}_2$ , and are separated by a distance  $\vec{r}$  is

$$U = \frac{1}{r^3} (\vec{\mu}_1 \cdot \vec{\mu}_2) - \frac{3}{r^5} (\vec{\mu}_1 \cdot \vec{r})(\vec{\mu}_2 \cdot \vec{r}) \quad (1)$$

The natural dipolar energy unit is that of two spheres at contact,  $u_d = \mu^2/D^3$ , which defines the reduced temperature,  $T^* = T/u_d$ . The maximal possible dipole-dipole attraction is  $-2u_d$ , obtained when the two spheres touch at nose-to-tail alignment, which is twice the attraction of antiparallel side-by-side dipoles (Fig. 1A). At low temperatures,  $T^* \ll 1$ , this strong anisotropy favors the linear aggregation of the spheres that are concatenated in the chains (Fig. 1B). The dipolar interaction is also long-range due to its  $r^{-3}$  decay. Nevertheless, in the absence of external magnetic field a thermodynamic limit exists (16) and the interaction becomes “nearly short range” for one-dimensional objects (17). Thus, we treat the chains as an ensemble of self-assem-

bling, “living” polymers that are free to break, reform, and exchange spheres.

In a certain regime of relatively low temperatures and densities, the chains will further organize and will interconnect via threefold junctions into a network. This branching occurs when it is energetically favorable to construct junctions from chain ends at the expense of the reduction of their translational entropy (Fig. 1C). Both topological defects, ends and junctions, cost dipolar interaction compared with the lower energy state of an infinite chain. However, the introduction of either kind of defect increases the entropy and is therefore favored at finite temperature. The energy cost of a free end,  $\epsilon_1$ , is larger than that of a junction,  $\epsilon_3$ . At low temperatures, this energy difference drives the formation of a network (18).

Our model of dilute dipolar fluids at low temperatures as self-assembling networks enables us to apply theoretical tools that were originally developed to treat living polymers (19), micellar solutions (20), and, recently, microemulsion networks (21, 22). The starting point of the model is the probability that a chain starts or terminates at a point  $\vec{r}$ ,  $\psi(\vec{r})$  (23). The probability for a chain crossing through  $\vec{r}$  is proportional to  $\psi(\vec{r})^2$ , because one may think of each monomer as the confluence of two chain ends. Within our mean-field model, it directly follows that the volume fraction of spheres scales like  $\phi \sim \psi^2$ . The concentration of ends is  $\psi$  multiplied by a Boltzmann factor that accounts for the energetic cost of an end defect,  $\rho_1 \sim \psi e^{-\epsilon_1/T^*} \sim \phi^{1/2} e^{-\epsilon_1/T^*}$ , where the defect energies are measured in units of  $u_d$ . Similarly, we find that the concentration of threefold junctions, that require the confluence of three ends, scales like  $\rho_3 \sim \psi^3 e^{-\epsilon_3/T^*} \sim \phi^{3/2} e^{-\epsilon_3/T^*}$ . Calculation of the free energy yields the standard result for systems gov-

erned by an interplay between the energy and entropy of topological defects. Each defect, whether it is a threefold junction or an end, contributes  $-k_B T$  (where  $k_B$  is the Boltzmann constant) to the free energy density (24)

$$f = -\rho_1 - \rho_3 + 1/2\phi^2 = - (2\phi)^{1/2} e^{-\epsilon_1/T^*} - 1/3(2\phi)^{3/2} e^{-\epsilon_3/T^*} + 1/2\phi^2 \quad (2)$$

where the third term accounts for the excluded volume repulsion between chains. Examining the osmotic pressure,  $p = \phi^2 \partial_\phi (f/\phi) = 1/2\phi^2 + 1/2(\rho_1 - \rho_3)$ , we find two opposing, topologically induced thermodynamic forces, a repulsion due to ends and an attraction due to junctions.

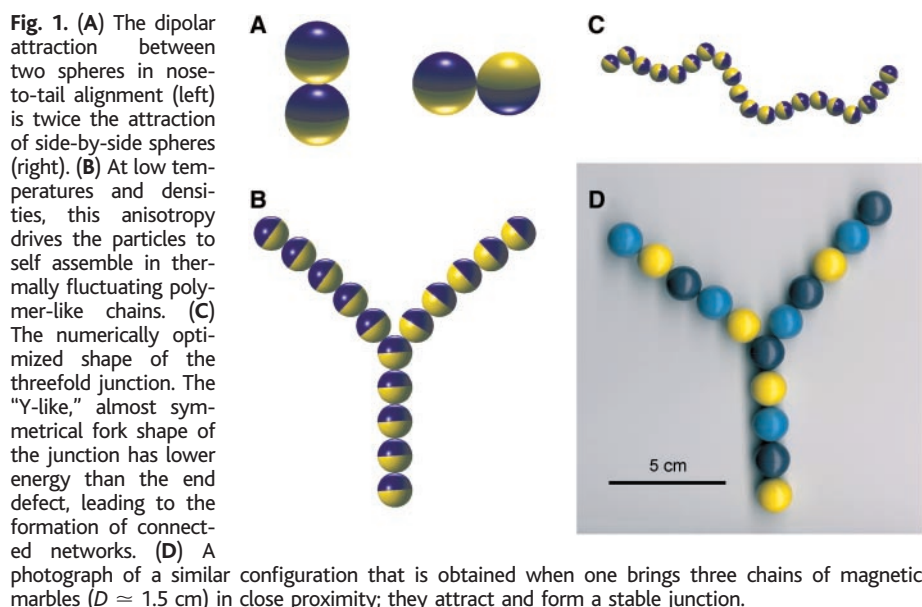
The dipolar fluid phase separates when the attraction of the dipolar junctions overcomes the repulsion due to ends and the excluded volume entropy loss. This phase separation occurs only below a critical temperature,  $T_c^*$ , located at the point where the coexistence curve meets the spinodal curve, the boundary of thermodynamic stability,  $\partial_\phi^2 f = 0$  (Fig. 2). Analysis of the free energy yields the critical temperature and volume fraction

$$T_c^* = \frac{\epsilon_1 - 3\epsilon_3}{3 \ln 3 - 2 \ln 2},$$

$$\ln \phi_c = - \frac{\epsilon_1(2 \ln 3 - \ln 2) - \epsilon_3 \ln 2}{\epsilon_1 - 3\epsilon_3} \quad (3)$$

The critical point has a remarkable topological significance. In analyzing  $f$  we find that the number of ends and junctions are equal  $\rho_1 = \rho_3$  at the critical point, which is thus a point of connectivity transition in the system (25, 26).

Indeed, the dipolar fluid separates into two isotropic phases, but the nature of the “liquid” and “gas” phases is different from



that of simple fluids. The basic “particles” in our model are not the individual dipolar spheres but the topological defects—the network junctions and free ends. Whereas the free energy of an individual sphere saturates to an almost constant value due to the strong dipolar attraction in the chains, the global structure and thermodynamics are governed by the entropy of the defects in accord with the isotherms of Camp *et al.*, which exhibit approximately constant free energy per sphere over almost one decade of increasing density in the regime of phase separation. The liquid-gas transition is, therefore, analogous to the demixing of a binary fluid consisting of junctions and ends. In the low density “gas” there are more ends than junctions ( $\rho_1 > \rho_3$ ) whereas the high density “liquid” is dominated by junctions ( $\rho_1 < \rho_3$ ). Hence, the liquid network is connected in the sense discussed above, whereas the gas is composed of disconnected chains. In the phase diagram, these two regions are separated by the connectivity transition line ( $\rho_1 = \rho_3$ ) (Fig. 2).

To further substantiate our proposal that the origin of the critical phase separation is a connectivity transition, we demonstrated that the energy cost of an end defect is indeed higher than that of a threefold junction. The estimates from the simulations of Camp *et al.* for the critical temperature and volume fraction are  $T_c^* \approx 0.15 - 0.16$  and  $\phi_c \approx 0.05 - 0.07$ , which correspond to defect energies of  $\epsilon_1 \approx 0.67$  and  $\epsilon_3 \approx 0.12$ , respectively (Fig. 2). We then compared these values to numerical estimates. The end energy cost is simply half the energy required to cut a continuous chain. Within the nearest neighbor approximation, this energy is  $\epsilon_1 = 1$ , and the upper limit obtained for straight, infinite chain is  $\epsilon_1 = \zeta(2) \approx 1.65$ . The excess energy and the

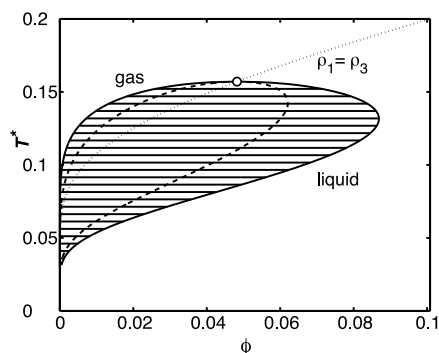


**Fig. 2.** The phase diagram of the dipolar network calculated for defect energies of  $\epsilon_1 = 0.67$  and  $\epsilon_3 = 0.12$ . At the critical point (circle), the coexistence curve (thick solid line), the phase stability boundary (dashed line), and the connectivity transition (dotted line) meet. The lines denote the coexistence of the end-rich “gas” with the junction-rich “liquid.” At low temperatures, the coexistence region narrows to very low densities.

“Y-like” fork shape of the optimal threefold junction are calculated by numerical minimization (Fig. 1C). A similar shape is obtained when one assembles three chains of magnetic marbles ( $D \approx 1.5$  cm) that form an energetically stable junction (Fig. 1D). Upon its formation, the junction gains one additional bond but loses more energy due to deviations from the optimal nose-to-tail alignment. This tunable balance results in a junction energy, which is lower than the end energy, as required. The estimate for the junction energy,  $\epsilon_3 \approx 0.2 - 0.5$ , reflects the analytical difficulties in minimizing the long-range dipolar interaction among the three finite, thermally fluctuating branches. The lower limits for  $\epsilon_1$  and  $\epsilon_3$  yield reasonable critical parameters,  $T_c^* \approx 0.20$  and  $\phi_c \approx 0.03$ , whereas the upper limits give an unrealistically small critical density.

The densities of both junctions and ends

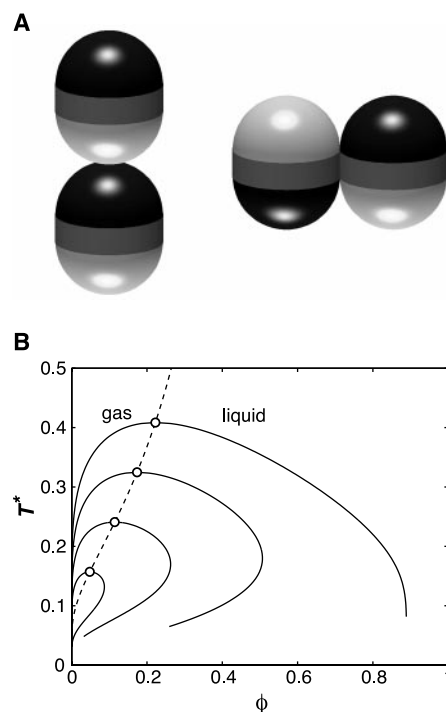


**Fig. 3.** (A) The sphero-cylindrical particles are composed of two hemispheres of diameter  $D$  separated by a cylinder of length  $L$ . The interaction energies of optimal sphero-cylinders ( $L/D \approx 1/4$ ) at nose-to-tail and side-by-side alignments are equal, which reduces the defect energies and leads to isotropic aggregation and a critical phase separation similar to that of isotropic fluids. (B) A similar effect is achieved by the introduction of a short-range attraction,  $\delta$ . The series of the calculated coexistence lines (solid) shows the progression, as the contact energy is increased (for  $\delta = 0, 0.08, 0.16, 0.24$ ) from the reentrant coexistence curve (lowest value of  $T_c^*$ ) to a parabolic shape, typical to isotropic fluids (highest value of  $T_c^*$ ). The dashed line follows the trajectory of the critical point.

decrease exponentially with decreasing temperature, leading to exponentially longer branches. The junction density,  $\rho_3 \sim e^{-\epsilon_3/T^*}$ , decreases slower than the end density,  $\rho_1 \sim e^{-\epsilon_1/T^*}$ , due to the lower defect energy. Therefore, in the proximity of the critical point, the junction attraction overcomes the end repulsion and the coexistence region expands. As temperature is further decreased, there are not enough junctions to balance by their attraction the excluded volume repulsion and the coexistence region narrows to very low densities (Fig. 2). This reentrance might be masked by the coexistence of the low-density gas with a solid-like phase or a high-density magnetic liquid (27). At low temperatures, we predict that the thermodynamically stable structure is that of a dilute network with many junctions and hardly any ends, in accord with the branched structures exhibited in simulations (4, 6). A crucial test of our model in experiment or simulation may be the observation of dipolar networks in the vicinity of the critical point in both coexisting phases (22).

The LGT of dipolar hard spheres is difficult to observe in simulations due to the small scales of density and entropy and the long relaxation times that stem from anisotropic chaining (28). One can overcome the strong anisotropy with the use of spherocylindrical particles composed of two hemispheres of radius  $D$  separated by a cylinder of length  $L$  (Fig. 3A). In this system, the degree of anisotropy of the nearest-neighbor interaction can be tuned by varying the aspect ratio  $L/D$ . At the optimal aspect ratio,  $L/D = 2^{1/3} - 1 \approx 1/4$ , the interaction energies of the nose-to-tail and side-by-side alignments become equal. As a result, the defect energies are reduced to  $\epsilon_1 \approx \zeta(2)/4 \approx 0.41$  and  $\epsilon_3 \approx -0.10$ . The negative junction energy indicates that the proliferating junctions are no longer thermal defects but the dominant structural element, so our picture does not apply. The attractive interaction, which is proportional to number junctions, is also amplified and the resulting LGT occurs more easily. The optimal sphero-cylinders retain the ability to cluster isotropically in three-dimensional aggregates like simple liquid particles, as seen in simulations (29). As the aspect ratio  $L/D$  shifts from its optimal value, the energy of the junctions increases, which exponentially decreases their number, and the phase separation eventually disappears. In the phase diagram, this nonmonotonic behavior is manifested by the appearance of reentrant two-phase coexistence “islands” (28, 29).

A similar enhancement of junction formation may be achieved by the introduction of a short-range attraction. Junctions ac-

quire an additional contact point whereas ends lose one when chains are broken. Accounting for the contribution of the cohesive energy,  $\delta$  (in units of  $u_d$ ) the defect energies shift like  $\epsilon_3 \rightarrow \epsilon_3 - 1/2\delta$  and  $\epsilon_1 \rightarrow \epsilon_1 + 1/2\delta$ . In particular, the critical temperature increases like  $T_c^* \rightarrow T_c^* + 1.05\delta$  and the reentrant coexistence curve evolves to a parabolic shape, typical of isotropic fluids (Fig. 3B). The crucial influence that the shape of the particles, their short-range interaction, and polydispersity have on their phase behavior can therefore be tested by measurement of the shape of the coexistence curve.

References and Notes

1. R. E. Rosensweig, *Science* **271**, 614 (1996).
2. T. C. Halsey, *Science* **258**, 761 (1992).
3. Of course, if enough isotropic attraction is added (e.g., van der Waals dispersion interaction), the usual isotropic three-dimensional aggregation is restored, and the resulting LGT does occur. However, the interesting and controversial point is whether phase separation can be driven by the dipolar interaction alone.
4. M. E. van Leeuwen, B. Smit, *Phys. Rev. Lett.* **71**, 3991 (1993).
5. M. J. Stevens, G. S. Grest, *Phys. Rev. Lett.* **72**, 3686 (1994).
6. D. Levesque, J. J. Weis, *Phys. Rev. E* **49**, 5131 (1994).
7. J. M. Tavares, J. J. Weis, M. M. Telo da Gama, *Phys. Rev. E* **59**, 4388 (1999).
8. P. G. de Gennes, P. A. Pincus, *Phys. Kondens. Mater.* **11**, 189 (1970).
9. A. P. Gast, C. F. Zukoski, *Adv. Colloid Interface Sci.* **30**, 153 (1989).
10. R. P. Sear, *Phys. Rev. Lett.* **76**, 2310 (1996).
11. R. van Roij, *Phys. Rev. Lett.* **76**, 3348 (1996).
12. Y. Levin, *Phys. Rev. Lett.* **83**, 1159 (1999).
13. P. J. Camp, J. C. Shelley, G. N. Patey, *Phys. Rev. Lett.* **84**, 115 (2000).
14. E. Dubois, V. Cabuil, F. Boué, R. Perzynski, *J. Chem. Phys.* **111**, 7147 (1999).
15. In their system, the particles are relatively small and the resulting dipolar interactions are weak. The formation of long chains is thus not likely, and our model of defect-induced phase separation may not apply.
16. S. Banerjee, R. B. Griffiths, M. Widom, *J. Stat. Phys.* **93**, 109 (1998).
17. This may be demonstrated by considering one spherical particle that belongs to an infinite, straight chain. The interaction of one sphere with the rest of the chain is

$$-2u_d \sum_{n=1}^{\infty} n^{-3} = -2u_d \zeta(3)$$

which is only  $\zeta(3) - 1 \approx 20\%$  larger than the interaction of the sphere with its two nearest neighbors,  $-2u_d$ .

18. Although junctions of even higher coordination number are also possible, they occur very rarely due to their higher energetic cost and lower entropy.
19. J. C. Wheeler, P. Pfeuty, *J. Chem. Phys.* **74**, 6415 (1981).
20. T. J. Drye, M. E. Cates, *J. Chem. Phys.* **96**, 1367 (1992).
21. T. Tlusty, R. Menes, S. A. Safran, R. Strey, *Phys. Rev. Lett.* **78**, 2616 (1997).
22. A. Bernheim-Grosswasser, T. Tlusty, S. A. Safran, Y. Talmon, *Langmuir* **15**, 5448 (1999).
23. P. G. de Gennes, *Scaling Concepts in Polymer Physics* (Cornell Univ. Press, Ithaca, NY, 1979), chaps. IX–X.
24. Minimizing the ideal-gas free energy of noninteracting defects,  $f_d = k_B T \rho_d (\ln \rho_d - 1) + \rho_d \epsilon_d$ , where  $\rho_d$  is the density of the defects and  $\epsilon_d$  their energy cost, one finds the optimal density  $\rho_d^* = e^{-\epsilon_d/k_B T}$  and the minimal free energy,  $f_d^* = -k_B T \rho_d^*$ .
25. Thinking of the self-assembling chains as the edges of a graph whose vertices are either junctions or ends, one finds that the density of vertices is  $v = \rho_1 + \rho_3$  whereas the density of edges is  $e =$

$1/2\rho_1 + 3/2\rho_3 = v + 1/2(\rho_1 - \rho_3)$ . This implies that at the critical point  $e = v = 2\rho_1 = 2\rho_3$ , the minimal graph connecting  $v$  vertices, a tree with  $e = v$  edges, becomes thermodynamically feasible.

26. T. Tlusty, S. A. Safran, R. Strey, *Phys. Rev. Lett.* **84**, 1244 (2000).
27. K. Sano, M. Doi, *J. Phys. Soc. Jpn.* **52**, 2810 (1983).
28. J. C. Shelley, G. N. Patey, D. Levesque, J. J. Weis, *Phys. Rev. E* **59**, 3065 (1999).

29. S. C. McGrother, G. Jackson, *Phys. Rev. Lett.* **76**, 4183 (1996).

30. We acknowledge fruitful discussions with J. Klein, R. E. Rosensweig, P. A. Pincus, and A. Zilman and support from The Israel Science Foundation center on Self-Assembly and the donors of the Petroleum Research Fund, administrated by the American Chemical Society.

9 August 2000; accepted 22 September 2000

# Macroscopic Fibers and Ribbons of Oriented Carbon Nanotubes

Brigitte Vigolo,<sup>1</sup> Alain Pénicaud,<sup>1</sup> Claude Coulon,<sup>1</sup> Cédric Sauder,<sup>2</sup> René Pailier,<sup>2</sup> Catherine Journet,<sup>3\*</sup> Patrick Bernier,<sup>3</sup> Philippe Poulin<sup>1†</sup>

A simple method was used to assemble single-walled carbon nanotubes into indefinitely long ribbons and fibers. The processing consists of dispersing the nanotubes in surfactant solutions, recondensing the nanotubes in the flow of a polymer solution to form a nanotube mesh, and then collating this mesh to a nanotube fiber. Flow-induced alignment may lead to a preferential orientation of the nanotubes in the mesh that has the form of a ribbon. Unlike classical carbon fibers, the nanotube fibers can be strongly bent without breaking. Their obtained elastic modulus is 10 times higher than the modulus of high-quality bucky paper.

Theoretical predictions (1, 2) and measurements on individual objects (3–5) suggest that single-walled carbon nanotubes (SWNTs) (6) could form the basis of materials with exceptional mechanical and electromechanical properties. Despite their intrinsic rigidity and high anisotropy, the currently available macroscopic forms of SWNTs are isotropic and rather fragile. These forms mainly consist of raw powder-like materials originating from synthesis (7, 8), suspensions in solvents (9), and thin mats, known as bucky paper, obtained by drying SWNT suspensions (10). Processing nanotubes on macroscopic scales to obtain materials with more practical uses is a major challenge. Here we report a simple and versatile approach that can create rigid fibers and ribbons of preferentially oriented SWNTs (11). Our processing consists of dispersing the nanotubes in surfactant solutions and then recondensing the nanotubes in the stream of a polymer solution. In contrast to most ordinary carbon fibers, SWNT fibers can be strongly bent and even tightly tied without breaking. Although they are still weak under tension, these recently obtained SWNT

fibers are already 10 times stronger than high-quality bucky paper, the main macroscopic form of SWNT nanotubes used so far (12).

The raw material we used was produced with the electric-arc technique (8). This technique produces SWNTs in the form of bundles of a few nanotubes, along with a certain fraction of carbon impurities and catalysts. This material was sonicated in aqueous solutions of sodium dodecyl sulfate (SDS), a surfactant that adsorbs at the surface of the nanotube bundles. At low surfactant concentrations, large and dense clusters of the initial material were still found after sonication. The amount of surfactant was too low to produce an efficient coating and induce electrostatic repulsions that could counterbalance van der Waals attractions (13). At higher SDS concentrations, black and apparently homogeneous suspensions were obtained. These suspensions did not coarsen or phase-separate macroscopically over several weeks. However, as revealed by optical microscopy (Fig. 1), dielectric measurements, and electron microscopy of freeze-fractured samples, these systems can in fact exhibit distinct phases. At intermediate concentrations of SDS, SWNTs were homogeneously dispersed and formed a single phase. The viscosity of these systems was almost that of pure water. In this regime, the electrostatic repulsion provided by adsorbed surfactants stabilized the nanotubes against van der Waals attraction. However, at higher SDS concentrations, a texture that reflected the formation of light clusters was observed. The clusters, which did not coarsen over several weeks,

<sup>1</sup>Centre de Recherche Paul Pascal/CNRS, Université Bordeaux I, Avenue Schweitzer, 33600 Pessac, France. <sup>2</sup>Laboratoire des Composites Thermostructuraux, Allée de la Boétie, 33600 Pessac, France. <sup>3</sup>Groupe de Dynamique des Phases Condensées, Université de Montpellier II, 34095 Montpellier, France.

\*Present address: Université Claude Bernard, Lyon I, 43 boulevard du 11 novembre 1918, 69622 Villeurbanne, France.

†To whom correspondence should be addressed. E-mail: poulin@crpp.u-bordeaux.fr